Coincidence measurements of intermediate mass fragments produced in ^{32}S-induced reactions on Ag at $E/A = 22.5$ MeV

D. J. Fields, W. G. Lynch, T. K. Nayak, M. B. Tsang, C. B. Chitwood, C. K. Gelbke, R. Morse,* and J. Wilczynski†
National Superconducting Cyclotron Laboratory, Michigan State University, East Lansing, Michigan 48824

T. C. Awes, R. L. Ferguson, F. Plasil, F. E. Obenshain, and G. R. Young
Oak Ridge National Laboratory, Oak Ridge, Tennessee 37830
(Received 28 February 1986)

Single- and two-particle inclusive cross sections for the production of light nuclei and intermediate mass fragments, $3 \leq Z \leq 24$, were measured at angles well beyond the grazing angle for ^{32}S-induced reactions on Ag at 720 MeV. Information about fragment multiplicities and reaction dynamics was extracted from measurements of light particles, intermediate mass fragments, and targetlike residues in coincidence with intermediate mass fragments. Incomplete linear momentum transfer and non-compound-particle emission are important features of collisions producing intermediate mass fragments. About half of the incident kinetic energy in these collisions is converted into internal excitation. The mean multiplicity of intermediate mass fragments is of the order of 1. Particle correlations are strongly enhanced in the plane which contains the intermediate mass fragment and the beam axis.

I. INTRODUCTION

The emission of low energy intermediate mass fragments, $3 \leqq Z_f \lesssim 25$, in processes distinct from fission is recognized to be a phenomenon characteristic of energetic proton-nucleus[1-7] and nucleus-nucleus collisions.[8-16] The energy spectra for these fragments typically exhibit broad maxima at energies slightly less than the exit channel Coulomb barriers and exponential slopes at higher energies. In general, the angular distributions are isotropic in the laboratory only at relativistic bombarding energies; for intermediate energies, the angular distributions are forward peaked, indicating that some emission occurs prior to the attainment of statistical equilibrium in the composite system.[4,11-15] The cross sections increase with bombarding energy;[4,11] in proton induced reactions they increase until $E_p \approx 5$ GeV, at which point they reach a limiting value.[4] They are characterized[5-7,11] by an approximate power-law dependence on fragment mass, $\sigma(A_f) \propto A_f^{-\tau}$, in both proton and heavy-ion induced reactions.

At present, there is no consensus concerning the origin of these fragments. The power law behavior of the mass yield distributions has been interpreted[5-7,17] in terms of statistical clustering[18] near the critical point in the liquid-gas phase diagram of nuclear matter. However, this interpretation is disputed.[19,20] Other models have been based on the assumption of thermodynamic disassembly[13,21-23] or the cold shattering[14,24-26] of the composite system, raising the possibility of relatively high fragment multiplicities in reactions with relatively small cross sections. Alternatively, statistical models of compound nucleus decay have been generalized[12,14,27-30] to account for the emission of intermediate mass fragments. These models are applicable at lower energies, at which sequential decay processes dominate.[12,16,31] At intermediate energies, they predict low fragment multiplicities.[14,29]

Until now, these models were principally compared with single particle inclusive data; each of them has achieved a certain degree of success in these comparisons. Critical judgments or improvements of the various models can be expected only in light of more restrictive measurements. In this paper we explore the statistical and dynamical aspects of intermediate mass fragment emission in ^{32}S-induced reactions on Ag at $E/A = 22.5$ MeV through measurements of intermediate mass fragments in coincidence with nonequilibrium light particles and heavy reaction residues. The intermediate mass fragments are detected at angles significantly larger than the grazing angle in order to reduce contributions from quasielastic peripheral processes. Both sets of coincidence measurements provide information about the relative importance of binary and multifragmentation emission mechanisms. Coincidence measurements with heavy recoils provide information about the momentum transfer and the inelasticity of the reactions. Coincidence measurements with nonequilibrium light particles provide information on the associated particle multiplicities as well as on the reaction dynamics.

In this paper we have deliberately avoided discussing the data in the context of a specific model, so that the essential features of the data are not confused with model dependent conclusions. The paper is organized as follows: Experimental details are given in the following section. In Sec. III single particle inclusive data are presented. Correlations between energetic light particles and light intermediate mass fragments are discussed in Sec. IV. Estimates of associated particle multiplicities are given in Sec. V. Coincidence measurements between low energy residual nuclei and intermediate mass fragments are presented in Sec. VI. Our conclusions are summarized in Sec. VII.

II. THE EXPERIMENT

The experiment was performed at the Holifield Heavy-Ion Research Facility at Oak Ridge National Laboratory. Self-supporting Ag targets were bombarded by ^{32}S ions of 720 MeV incident energy. Two independent sets of measurements were made: (1) Correlations between light particles and intermediate mass fragments were measured with a 3.2 mg/cm^2 target. This relatively thick target was used because of low coincidence cross sections and limits these coincidence measurements to fragments, $Z_f \leqq 7$. (2) Velocity distributions of heavy reaction residues emitted in coincidence with intermediate mass fragments were measured with a 0.75 mg/cm^2 target. This target was also used for the measurements of the single particle inclusive cross sections.

A schematic drawing of the experimental geometry is shown in Fig. 1. α particles and intermediate mass fragments, $3 \leqq Z_f \leqq 24$, were detected with three ΔE-ΔE-E detector telescopes, with individual solid angles of 8 msr. These telescopes were located at the azimuthal angle of $\phi = 0°$ and at the polar angles of $\theta = 27.5°$, 40°, and 52.5° with respect to the beam axis. Each telescope consisted of a 10 cm deep Frisch grid ion chamber followed by 400 μm and 5 mm thick silicon detectors. The solid state detectors were calibrated with a charge injecting pulser and with α particles from a ^{244}Cm source. The ion chambers were operated at a pressure of 150 Torr using a 90% Ar + 10% CH_4 gas mixture. They were calibrated with heavy ions of known energy, using published energy loss tables.[32] The energy calibrations are accurate to 5%.

The velocities of coincident heavy reaction residues were measured with a position sensitive parallel plate detector with an active area of 10.5 cm × 10.5 cm. This detector was located at a distance of 50.2 cm from the target; its azimuthal angle was $\phi = 180°$. A total angular range in the reaction plane, $5° \leqq \theta \leqq 23°$, was covered in three measurements with the detector centered at $\theta = 11°$, 16°, and 22°; these measurements span the angles expected for binary decay following full momentum transfer. The detector subtended a 12° opening angle perpendicular to the plane defined by the beam axis and the three intermediate mass fragment telescopes. The time-of-flight measurements were calibrated via the cyclotron radio frequency and the time of flight of elastically scattered beam particles. The velocity vectors of the heavy residual nuclei are accurate to within 5% and 1°.

Light particles, p, d, t, and α, were detected by five ΔE-E telescopes, each consisting of a 400 μm thick silicon detector and a 10 cm thick NaI(Tl) scintillator. Three of these telescopes were placed at the azimuthal angle of $\phi = 90°$ and at the polar angles of $\theta = 40°$, 70°, and 130°; two telescopes were positioned at $\phi = 180°$ and at $\theta = 40°$ and 70°. They subtended solid angles between 22 and 65 msr. The NaI detectors were calibrated with recoil protons produced via elastic scattering of ^{32}S ions from a polyethylene target. The calibrations are accurate to 5%. Coincident and downscaled singles events were recorded on magnetic tape and analyzed off line. The absolute normalizations of the cross sections are accurate to within 10%.

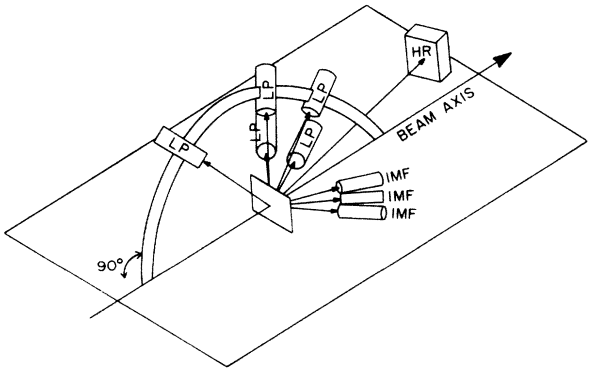

FIG. 1. Schematic drawing of the experimental setup. The intermediate mass fragment detectors at $\phi = 0°$ are labeled IMF. The light particle detectors, located at $\phi = 90°$ and 180°, are labeled LP. The position sensitive heavy residue detector at $\phi = 180°$ is labeled HR.

III. SINGLE PARTICLE INCLUSIVE DATA

The measured single particle inclusive cross sections are shown in Figs. 2–4. Both light particle and intermediate mass fragment inclusive cross sections are forward peaked in the laboratory and center-of-mass rest frames, indicating the onset of emission prior to the establishment of thermal equilibrium in the composite system. The energy

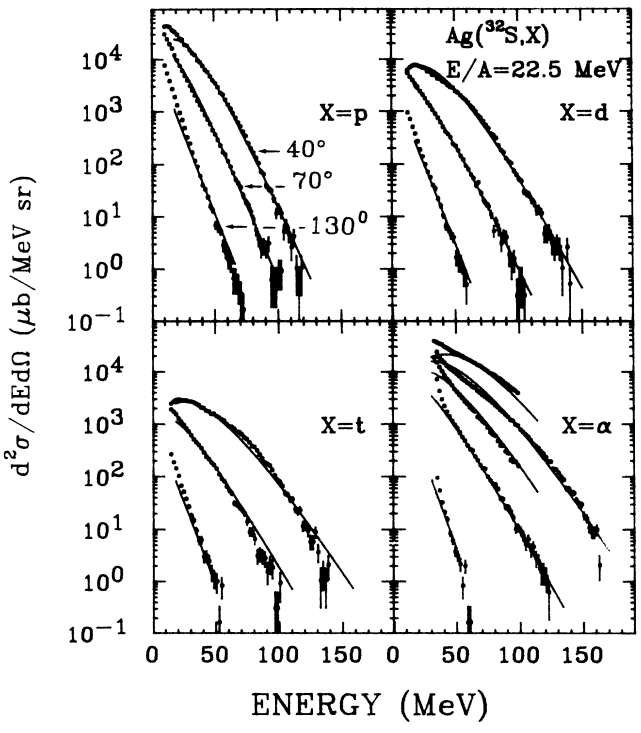

FIG. 2. Differential cross sections for p, d, t, and α particles emitted at the laboratory angles of 40°, 70°, and 130°. (For α particles, additional spectra were measured at 27.5° and 52.5°.) The solid lines correspond to fits with the parametrization described in Sec. III.

spectra for light particles (Fig. 2) exhibit the characteristic features and follow the systematic trends previously established for non-compound-light-particle emission in intermediate energy nucleus-nucleus collisions.[33,34] At present, however, there is insufficient experimental information to establish systematic dependences of intermediate mass fragment cross sections upon bombarding energy or the masses of the projectile, target, or emitted fragments.

To organize the present set of data and to provide reasonable extrapolations to unmeasured scattering angles, we fit our cross sections with a single parametrization, which models both a fusionlike and a nonequilibrium source, each emitting isotropically with a Maxwellian energy distribution in its respective rest frame. We must emphasize that the parametrization should not be interpreted in terms of the sequential decay of two well defined sources. The emission of intermediate mass fragments is a much more complicated process involving a continuum of "sources" from the quasielastic regime to the compound nucleus. However, the present single particle data do not justify a larger parameter space than the restricted two source space used here. In addition, this parametrization facilitates the formation of a qualitative picture of the timescale for emission as compared to the timescale for the dissipation of the entrance channel kinetic energy into intrinsic degrees of freedom.

We formulate this parametrization in a rest frame $O_{\rm eq}$ which moves with a velocity $v_{\rm eq}$ with respect to the laboratory frame. This velocity is chosen to be characteristic of fusionlike residues. In this frame the cross sections are given by

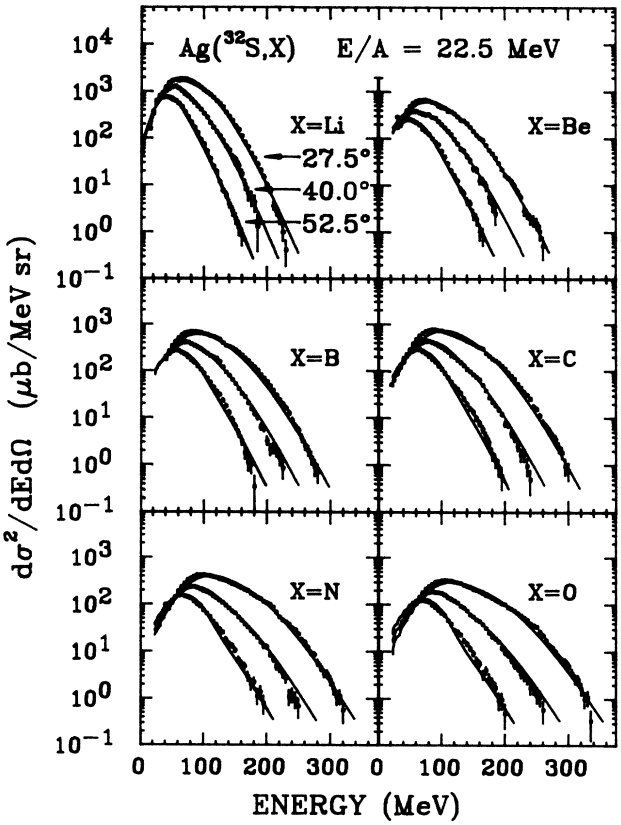

FIG. 3. Differential cross sections for Li, Be, B, C, N, and O nuclei measured at 27.5°, 40°, and 52.5°. The solid curves correspond to fits with the parametrization described in Sec. III.

$$\tilde{\sigma}'_x(\theta',E')=\frac{d^2\sigma'_x}{dE'd\Omega'}=\int\left[N_{\rm eq}(E'-V_C)\exp\left[-\frac{E'-V_C}{T_{\rm eq}R}\right]+N_f[(E'-V_C)E_f]^{1/2}\exp\left[-\frac{E_f}{T_f}\right]\right]$$
$$\times(2\pi w_x^2)^{-1/2}\exp\left[-\frac{(V_C-RV_x)^2}{2w_x^2}\right]dV_C\ , \tag{1}$$

with

$$E_f=E'-V_C+E_d-2[(E'-V_C)E_d]^{1/2}\cos\theta'$$

and

$$E_d=\tfrac{1}{2}M_x(v_f-v_{\rm eq})^2\ .$$

Here, the factor

$$R=(M_p+M_T-M_x)/(M_p+M_T)$$

is due to momentum conservation, where M_p, M_T, and M_x denote the masses of the projectile, target, and fragment, respectively; E' is the energy of the fragment in the frame $O_{\rm eq}$; v_f is the velocity of the fast, nonequilibrium source with respect to the laboratory; and N_f and T_f ($N_{\rm eq}$ and $T_{\rm eq}$) are the normalization and "temperature" parameters which characterize the fast (slow) source. To avoid sharp cutoffs at low energies, Eq. (1) contains a weighted average over a Gaussian distribution of Coulomb barriers V_C. The parameters V_x and w_x are the mean and the standard deviation of this distribution. Comparison to experimental data is made after transforming Eq. (1) to the laboratory rest frame to yield the laboratory cross sections $\tilde{\sigma}_x(\theta,E)$. We used the value $v_{\rm eq}=0.86\times v_0M_p/(M_p+M_T)$, where v_0 is the projectile velocity. This value is consistent with the systematics for linear momentum transfer observed in measurements on fissile targets.[35]

We have assumed that particles are emitted from the surface of both the equilibrium and nonequilibrium sources in our derivation of Eq. (1). Temperature parameters obtained under this assumption are approximately 10% lower than the corresponding parameters extracted with a parametrization which assumes volume emission.

In order to reduce the number of variable parameters, we used Coulomb widths of $w_x=2$, 4, 11, and 17 for $Z_x=1$, 2, 3, and $4\leq Z_x\leq 24$, respectively. The temperature parameter of the fusionlike source was fixed at $T_{\rm eq}=7$ MeV. This leaves $N_{\rm eq}$, N_f, v_f, T_f, and V_x as free parameters.

The resulting fits, shown as the solid lines in Figs. 2–4, are superior to fits with a single moving source.[14] The fit

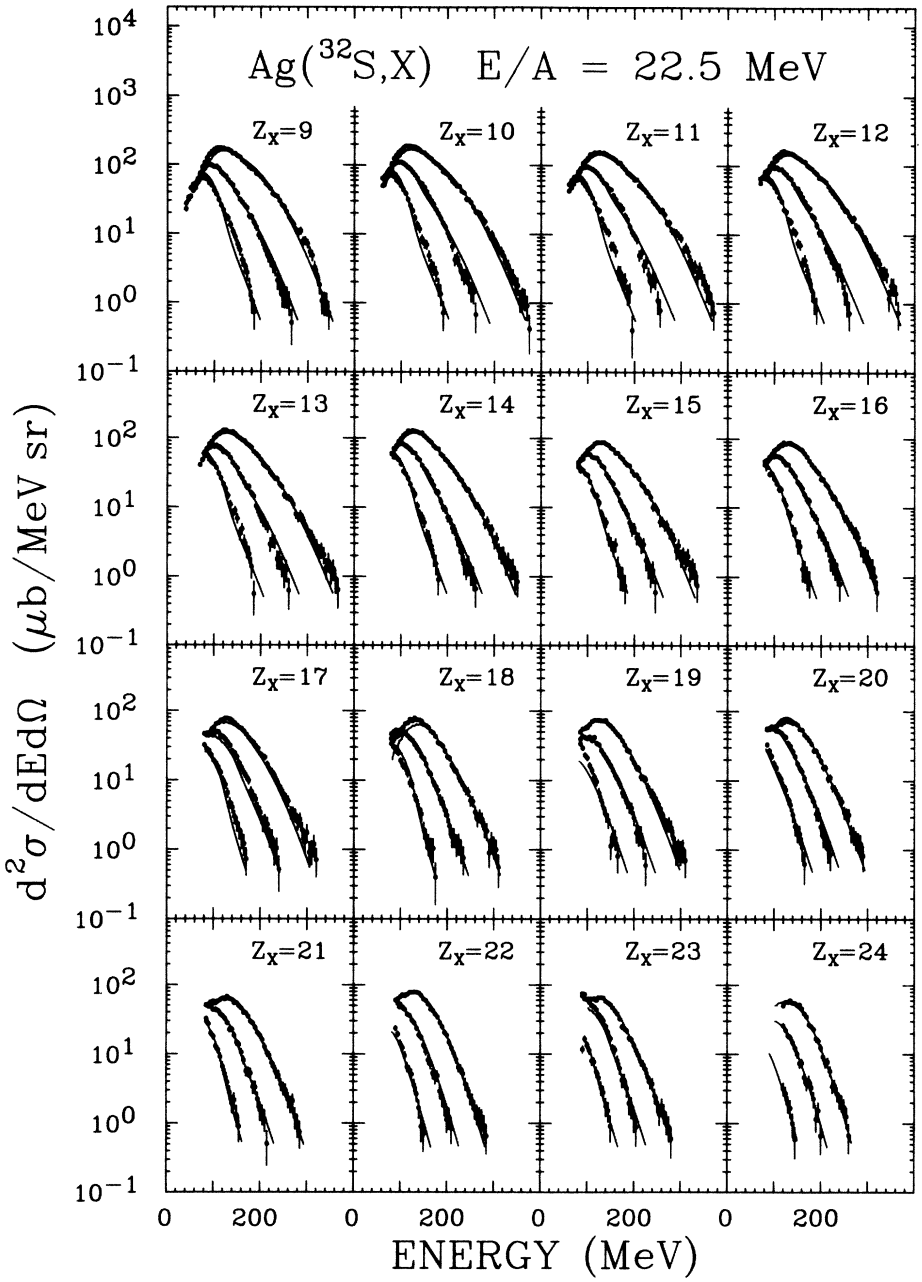

FIG. 4. Differential cross sections for nuclei, $9 \leq Z \leq 24$, measured at laboratory angles of 27.5°, 40°, and 52.5°. The solid curves correspond to fits with the parametrization described in Sec. III.

parameters are given in Table I. The relative contribution from the fusionlike source increases with increasing fragment mass, becoming the dominant contribution for $Z_x \geq 8$. The velocity of the nonequilibrium source decreases with fragment mass, rendering the spectral decomposition into two sources increasingly artificial for $Z_x > 13$. A decrease in the apparent source velocity with fragment mass is observed in heavy ion induced reactions whenever fragments with target rapidity are measured.[14,15,36] This suggests that the cross sections of heavier fragments may have sizable contributions from later, more equilibrated stages of the reaction.[14]

The temperature of the fast source remains relatively constant for fragments of charge $Z_x \leq 20$, at which point it begins to decrease. (This feature is also observed in fits with a single moving source.) A similar behavior has also been observed in ^{40}Ar induced reactions on ^{197}Au at higher bombarding energies.[13] It differs from reactions with lighter projectiles, where the "temperatures" decrease systematically over the entire range of fragment masses.[14,15,36]

Finally, the Coulomb barrier V_x is considerably smaller than the Coulomb barrier V_s between two touching spheres, possibly indicating emission from highly de-

TABLE I. The parameters resulting from the fits with Eq. (1). The parameter T_f is the temperature of the fast source; v_f/v_0 is the ratio of the velocity of the fast source to that of the projectile; N_f and N_{eq} are the normalization constants for the fast and equilibrated sources; V_x is the mean Coulomb barrier and V_s is the Coulomb barrier calculated for touching spheres of radius $R=1.44\times A^{1/3}$; σ_f and σ_{eq} are the integrated cross sections from each source.

X	T_f (MeV)	v_f/v_0	N_f	N_{eq}	V_x/V_s	σ_f (mb)	σ_{eq} (mb)
p	6.09	0.53	6610	600	0.4	3060	367
d	7.08	0.52	1650	320	0.4	1030	193
t	8.38	0.50	515	100	0.4	450	59
α	7.99	0.50	3320	790	0.4	2630	460
Li	8.36	0.55	278	280	0.73	240	152
Be	8.96	0.54	81.7	156	0.71	79.2	74.3
B	9.62	0.50	74.1	172	0.78	84.4	84.5
C	9.30	0.50	98.7	194	0.80	106	96.9
N	10.2	0.49	48.2	118	0.76	63.1	57.5
O	10.6	0.49	34.4	110	0.75	48.2	52.1
F	11.2	0.49	16.9	65.6	0.75	26.3	30.1
Ne	11.2	0.48	17.4	80.0	0.69	27.5	35.3
Na	11.7	0.46	13.2	70.2	0.69	22.7	36.5
Mg	11.8	0.43	12.5	73.8	0.68	21.6	30.2
Al	12.2	0.40	8.94	60.4	0.62	16.7	23.7
Si	11.7	0.38	9.34	64.2	0.61	15.9	24.2
P	11.4	0.36	7.04	43.7	0.55	11.5	15.8
S	11.3	0.34	6.69	45.2	0.55	10.8	15.7
Cl	10.0	0.34	7.49	40.0	0.45	9.29	12.6
Ar	10.7	0.32	6.47	38.5	0.50	9.30	12.1
K	11.2	0.31	5.37	40.5	0.47	8.40	11.9
Ca	10.4	0.29	7.60	39.7	0.45	10.0	10.7
Sc	9.72	0.30	5.94	46.0	0.47	6.96	12.3
Ti	9.18	0.27	14.0	20.0	0.36	14.0	4.57
V	9.89	0.26	6.24	45.9	0.42	7.43	10.4
Cr	8.59	0.26	13.6	5.0	0.32	11.6	1.0

formed systems or significant contributions from the sequential decay[37] of highly excited primary fragments.

Total cross sections for intermediate mass fragments were extrapolated by integrating Eq. (1) over energy and solid angle. These extrapolations are shown as open points in Fig. 5. The solid points in Fig. 5 represent cross sections $\langle d\sigma/d\Omega\rangle$ obtained by averaging the experimental data over scattering angle:

$$\left\langle \frac{d\sigma}{d\Omega} \right\rangle = \frac{\sum_i [d\sigma(\theta_i)/d\Omega]\Delta\Omega(\theta_i)}{\sum_i \Delta\Omega(\theta_i)} , \quad (2)$$

where $\Delta\Omega(\theta_i)=2\pi\sin\theta_i\Delta\theta$, and $\Delta\theta=12.5°$ is the angular separation of the fragment detectors. Both cross sections decrease smoothly with fragment charge and show no particular enhancement in the neighborhood of the projectile ($Z_x=16$), as would be expected at angles closer to the grazing angle. The elemental distributions in Fig. 5 fall off much more gradually with fragment charge than the yield distributions observed in proton induced reactions[3,5–7] or ^{12}C-induced reactions on Au and Ag.[11] Other factors besides the internal excitation energy of the composite system, such as collision dynamics and angular momentum, must play a major role in the emission process.

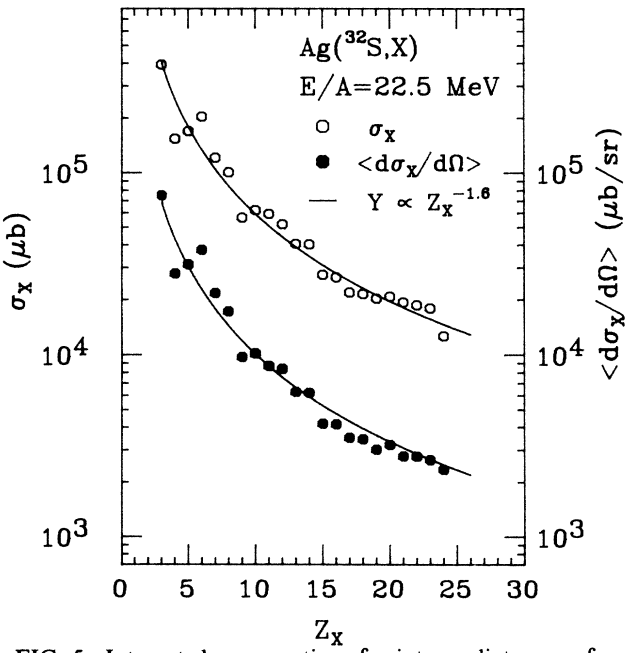

FIG. 5. Integrated cross sections for intermediate mass fragments. The open points represent the total cross sections extrapolated from the fits shown in Figs. 2 and 3. The solid points represent the differential cross section $\langle d\sigma/d\Omega\rangle$ averaged over the measured angular range. The solid curves correspond to a function $cZ^{-1.6}$, where c has been chosen to provide a reasonable overall normalization.

IV. CORRELATIONS BETWEEN INTERMEDIATE MASS FRAGMENTS AND LIGHT PARTICLES

In this section we will examine correlations between energetic light particles and light intermediate mass fragments, $3 \leqq Z_x \leqq 7$, at large relative angles.

Light particle energy spectra measured in coincidence with intermediate mass fragments are similar to those measured inclusively. This is illustrated in Fig. 6. The upper and lower parts of this figure show energy spectra of protons and α particles, respectively, measured at $\theta_y = 40°$ and 70°. Single particle inclusive spectra, shown as solid curves, are compared to spectra measured in coincidence with lithium (left hand side) and carbon fragments (right hand side), detected at $\theta_x = 27.5°$ and $\phi_x = 0°$. Coincidence spectra measured for $\phi_y = \phi_y - \phi_x = 180°$ (coplanar geometry, solid points) are nearly identical in shape to the singles spectra. Coincidence spectra measured for $\phi_y = \phi_y - \phi_x = 90°$ (out-of-plane geometry, open points) exhibit slightly steeper slopes. This difference in slope is more pronounced for α particle spectra than for proton spectra.

We examine the differences between coincidence and singles spectra in more detail by defining the spectrum ratio $R(E_y, \theta_y, \theta_x, \phi_y - \phi_x)$:

$$R(E_y, \theta_y, \theta_x, \phi_y - \phi_x) = \frac{\int dE_x \sigma_{yx}(E_y, E_x, \theta_y, \theta_x, \phi_y - \phi_x)}{\sigma_y(E_y, \theta_y)}, \quad (3)$$

where we use, for brevity,

$$\sigma_{yx} = \frac{d^4\sigma_{yx}}{dE_y d\Omega_y dE_x d\Omega_x} \quad \text{and} \quad \sigma_y = \frac{d^2\sigma_y}{dE_y d\Omega_y}.$$

Comparisons which utilize the spectrum ratio have the advantage of being relatively insensitive to uncertainties in energy calibrations and normalizations. Spectrum ratios for protons ($y = p$) and alpha particles ($y = \alpha$) are shown in Figs. 7 and 8, respectively. Spectra measured in coincidence with lithium and carbon nuclei are shown in the upper and lower parts of each figure. Solid and open points represent the spectrum ratios for $\phi_y = 180°$ and 90°, respectively. For $\phi_y = 180°$, the spectrum ratio is nearly constant, demonstrating the close similarity of the single-particle inclusive energy spectra to the coincidence spectra measured in the coplanar geometry. For $\phi_y = 90°$ the spectrum ratios tend to decrease with increasing light particle energy; they are also smaller than for $\phi_y = 180°$, indicating that coincident particles are preferentially emitted in a common plane containing the beam axis. This preference for coplanar emission becomes more pronounced as the mass of either of the two detected particles is increased. The slopes of the spectrum ratios correspond to differences in the temperature parameters which characterize the singles and coincidence spectra. The largest measured difference between these parameters is of the order of 10–15 %.

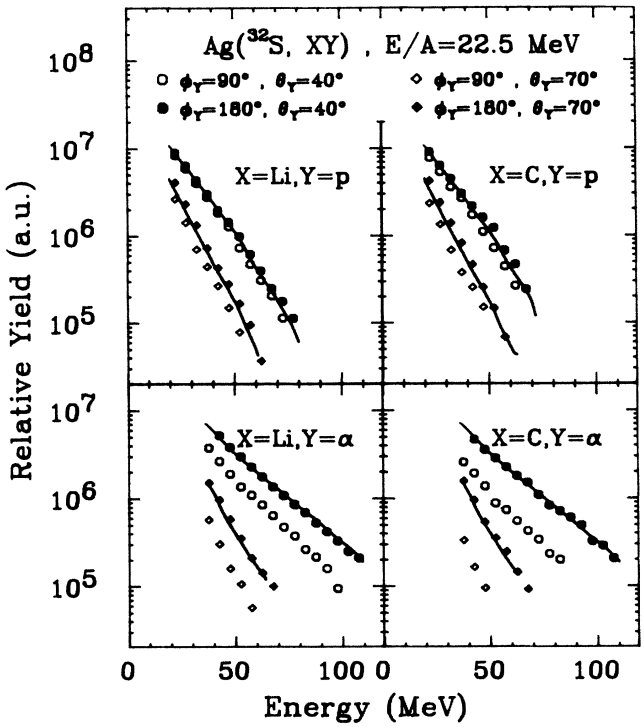

FIG. 6. Comparison between single particle inclusive spectra (solid curves) and spectra of light particles measured in coincidence with lithium fragments (left hand side) and carbon fragments (right hand side). The solid and open points refer to $\phi_y = 180°$ and 90°, respectively. Coincidence spectra measured at 40° and 70° are shown by circles and diamonds, respectively.

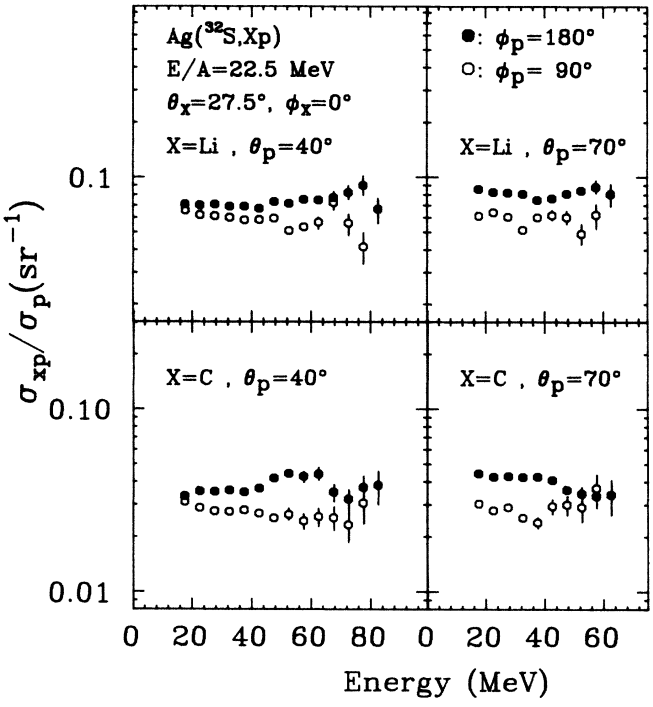

FIG. 7. The spectrum ratio of the coincidence and single particle differential cross sections, defined in Eq. (3), for protons in coincidence with Li (upper part) and C nuclei (lower part), as a function of energy. The spectra for protons detected at 40° and 70° are shown on the left and right hand sides of the figures, respectively. The solid and open points represent the in-plane and out-of-plane ratios, respectively.

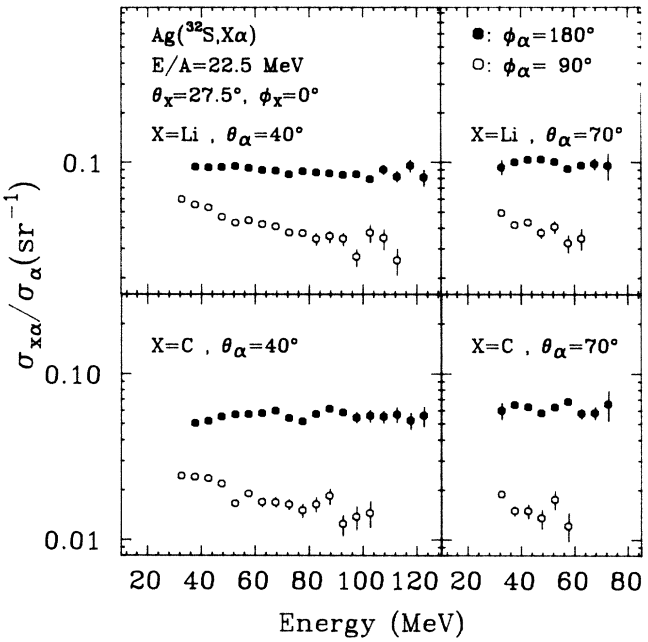

FIG. 8. The spectrum ratio of the coincidence and single particle differential cross sections, defined in Eq. (3), for α particles in coincidence with Li (upper part) and C nuclei (lower part), as a function of energy. The spectra for α particles detected at 40° and 70° are shown on the left and right hand sides of the figures, respectively. The solid and open points represent the in-plane and out-of-plane ratios, respectively.

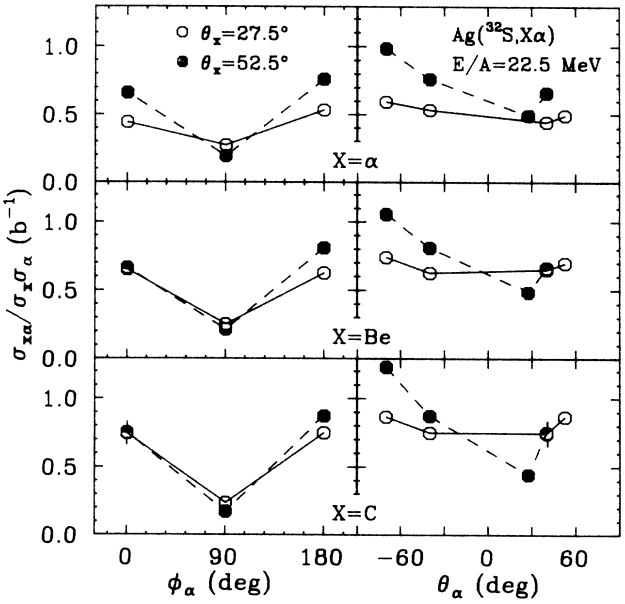

FIG. 9. Two-particle correlations, defined in Eq. (4), between intermediate mass fragments x and α particles. The left hand side depicts correlations for α particles detected at $\theta_\alpha=40°$ at three azimuthal angles ϕ_α. The intermediate mass fragment is detected at the polar angle θ_x and the azimuthal angle $\phi_x=0°$. The right hand side depicts in-plane correlations as a function of polar angle θ_α. Positive and negative values of θ_α correspond to $\phi_\alpha=0°$ and 180°, respectively. The lines are drawn to guide the eye.

The similarity of light particle spectra measured inclusively with those measured in coincidence with intermediate mass fragments indicates that intermediate mass fragments and non-compound light particles are emitted in similar types of reactions. It also suggests that the emission of these particles is largely independent of fragment emission, e.g., these light particles are not principally emitted in the sequential decay of binary reaction products. There is no evidence that the assumption of statistical emission is strongly violated.

The systematic dependence of the two particle inclusive cross section upon the masses and scattering angles of the two particles can be examined with great sensitivity in terms of the correlation function, $C(\theta_y,\theta_x,\phi_y-\phi_x)$, which is defined by

$$C(\theta_y,\theta_x,\phi_y-\phi_x) = \frac{\int_y\int_x dE_y dE_x \sigma_{yx}(E_y,E_x,\theta_y,\theta_x,\phi_y-\phi_x)}{\int_y\int_x dE_y dE_x \sigma_y(E_y,\theta_y)\sigma_x(E_x,\theta_x)}, \quad (4)$$

where the constraints bounding the integration of energy variables are given below. The sensitivity of the correlation function derives from the cancellation of the exponential dependences of the single- and two-particle inclusive cross sections upon energy and angle. Experimental uncertainties of the detector placement, solid angle, and energy calibration do not influence the correlation function since singles and coincidence data were taken simultaneously. As a consequence, subtle correlations arising from collision dynamics,[38,39] phase space constraints,[39–43] or contributions from single nucleon scattering processes[44,45] can be probed with a high degree of accuracy.

The correlation function can be strongly distorted by the sequential decay of particle unbound systems and by final state interactions, particularly when the relative momentum of the two particles is small.[37,46–54] In order to avoid such effects, we have excluded from the energy integrations those relative energies for which these effects are expected to be important. The correlations between α particles and light intermediate mass fragments shown in Figs. 9 and 10 are integrated for relative energies, $E_{\rm rel} > E_0$, where $E_0=6$, 7, 6, 9, 11, and 10 MeV for fragment charges of $Z=2$–7, respectively. This restriction influences the two particle correlations principally at small relative angles.

Examples of the angular correlations between light intermediate mass fragments and α particles ($y=\alpha$) are presented in Fig. 9. The left hand side of the figure shows correlations as a function of ϕ_α for α particles detected at $\theta_\alpha=40°$ and intermediate mass fragments detected at $\theta_x=27.5°$, $\phi_x=0°$ (open points) or $\theta_x=52.5°$, $\phi_x=0°$ (solid points). The integrations in the correlation function were performed over particle energies above the thresholds, $E_x/A_x > 5$ MeV and $E_\alpha > 40$ MeV. The azimuthal correlation function exhibits a pronounced minimum at

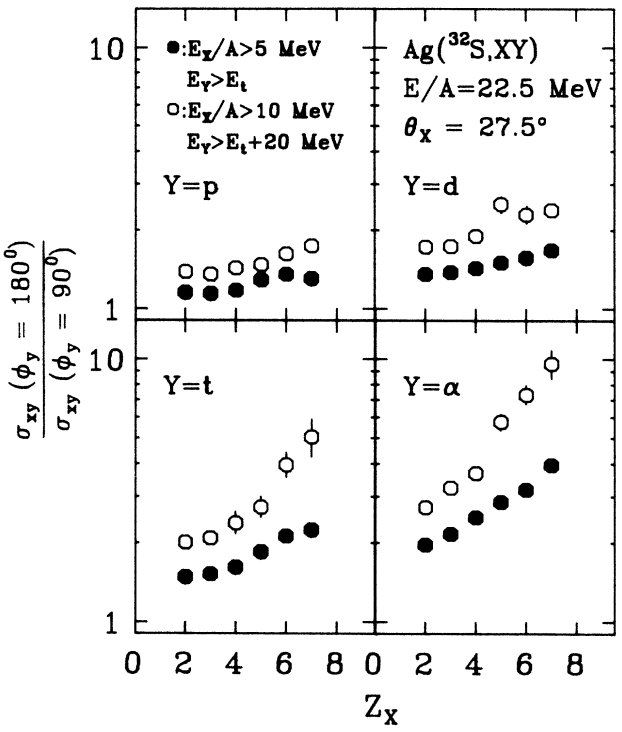

FIG. 10. Azimuthal asymmetries, defined in Eq. (5), for protons, deuterons, tritons and α particles detected in coincidence with intermediate mass fragments of element number Z_x. Light particles are emitted at the angles $\theta_y = 40°$ and $\phi_y = 180°$ or 90°; intermediate mass fragments are detected by $\theta_x = 27.5°$, $\phi_x = 0°$. The energy thresholds are given in the text; open points represent higher energy thresholds.

$\phi_\alpha = 90°$, corresponding to the strong preference for emission in a common reaction plane. The coincidence cross sections for emission to the same or to opposite sides of the beam axis are of similar magnitude. The minimum at $\phi_\alpha = 90°$ is more pronounced if the intermediate mass fragment is detected at the larger angle of $\theta_x = 52.5°$.

We characterize the enhanced emission in the reaction plane in terms of the azimuthal asymmetry A_ϕ, which is defined as the cross section ratio of in-plane and out-of-plane coincidences:

$$A_\phi = \frac{\sigma_{xy}(\phi_y = 180°)}{\sigma_{xy}(\phi_y = 90°)} = \frac{C(\theta_x = 27.5°, \theta_y = 40°, \phi_y - \phi_x = 180°)}{C(\theta_x = 27.5°, \theta_y = 40°, \phi_y - \phi_x = 90°)} . \quad (5)$$

The correlation functions C are defined in Eq. (4). The dependence of the azimuthal asymmetry on particle type is shown in Fig. 10. For the solid points the cross sections were integrated over the energies of $E_x/A_x > 5$ MeV and $E_y > E_t$ for intermediate mass fragments, x, and light particles, y, respectively. The light particle energy thresholds were $E_t = 15$, 20, 20, and 40 MeV for protons, deuterons, tritons, and α particles, respectively. The open points show the azimuthal asymmetries for fragments and light particles of higher energy, $E_x/A_x > 10$ MeV and $E_y > E_t + 20$ MeV. The azimuthal asymmetries increase with increasing mass of the coincident particles and become more pronounced with increasing particle energy. For correlations between high energy nitrogen ions and α particles, the in-plane to out-of-plane ratio is nearly 10.

The right hand side of Fig. 9 shows in-plane correlations between coincident α particles detected at θ_α and intermediate mass fragments detected at $\theta_x = +27.5°$ (open points) and at $\theta_x = +52.5°$ (solid points). Here, positive and negative values of θ_α correspond to the azimuthal angles $\phi_\alpha = 0°$ and $\phi_\alpha = 180°$, respectively. The approximate symmetry of these correlations about the beam axis indicates again that nonequilibrium light particles are not principally emitted in the sequential decay of the intermediate mass fragment or a heavy reaction residue.[55] The in-plane correlations decrease at forward angles. The effect is more pronounced when the intermediate mass fragment is emitted at a larger angle.

A decrease in the correlation at forward angles would occur if the singles spectra of light particles at forward angles contained significant contributions from peripheral breakup reactions which do not lead to the emission of low energy intermediate mass fragments. However, this effect alone does not explain the dependence of the correlation function on the emission angle θ_x of the intermediate mass fragment. Alternatively, strongly enhanced emission in the reaction plane will produce a dip in the correlation function at forward angles which becomes larger as the angle of the gating particle is increased. It may well be possible that the minimum of the in-plane correlation function at small angles is due to a combination of these two effects.

The azimuthal correlations are similar to those observed[39,42] for coincident light particles emitted in ^{16}O induced reactions on ^{197}Au at $E/A = 25$ MeV. Furthermore, light-particle fission-fragment coincidence measurements have demonstrated that light particles are preferentially emitted in the entrance channel scattering plane which is perpendicular to the entrance channel orbital angular momentum.[38] Therefore, it is likely that intermediate mass fragments, too, are preferentially emitted in this plane. The azimuthal correlations measured in Refs. 38, 39, and 42 could be understood in terms of a collective transverse motion in the reaction plane, upon which is superimposed the random motion of the individual light particles. The enhanced emission of particles in the entrance channel scattering plane has recently been explained[56] in terms of the Boltzmann-Uehling-Uhlenbeck theory[57,58] and was attributed to the collective motion of the nucleons in the attractive nuclear mean field. In its present formulation,[57,58] this theory does not predict self-consistent two-particle distributions or the emission of complex particles. Comparison of our data to such a microscopic theory is, therefore, not yet feasible. Nevertheless, it appears that the mean field dynamics is relevant to the interpretation of complex fragment emission in intermediate energy nucleus-nucleus collisions.

V. ASSOCIATED MULTIPLICITIES

It is useful to know the average multiplicities of particles in reactions producing intermediate mass fragments.

We have exploited the similarities between singles and coincidence spectra to estimate the multiplicity of particle y, associated with the emission of particle x, by

$$M_y = \frac{\int_x \int_y dE_x dE_y \sigma_{xy}(E_x,\theta_x,E_y,\theta_y)}{\int_x dE_x \sigma_x(E_x,\theta_x)} \times \frac{\tilde{\sigma}_y^{\text{tot}}}{\int_y dE_y \tilde{\sigma}_y(E_y,\theta_y)}, \quad (6)$$

where $\sigma_{xy}(E_x,\theta_x,E_y,\theta_y)$ is the experimental differential coincidence cross section for particles x and y, and $\sigma_x(E_x,\theta_x)$ is the experimental differential cross section for particle x. The integrals $\int_x dE_x$ and $\int_y dE_y$ extend over the experimental acceptances of the detectors. The total and differential cross sections for particle y, $\tilde{\sigma}_y^{\text{tot}}$ and $\tilde{\sigma}_y(E_y,\theta_y)$, are given by the parametrizations described in Sec. III. We estimate that the extrapolation over unmeasured angles introduces a model dependent uncertainty in the multiplicity estimates which could be as large as 50%.

The multiplicities of nonequilibrium light particles associated with the emission of Li, B, and C fragments of various momenta $\langle P_x \rangle$ detected at $\theta_x = 27.5°$ are deduced from the cross sections of coincident light particles detected at $\theta_y = 40°$. The estimates obtained from in-plane and out-of-plane coincidence cross sections are averaged. The resulting values are listed in Table II. At least ten nonequilibrium nucleons are emitted in the form of light particles, $Z \leq 2$, in collisions leading to the emission of intermediate mass fragments. (We assume that the multiplicities of nonequilibrium neutrons are identical to those for nonequilibrium protons.) If these nucleons are emitted with distributions which are similar to the corresponding single particle distributions, then they remove a total momentum of 1100 MeV/c and a total kinetic energy of about 160 MeV from the system.

The multiplicities of intermediate mass fragments associated with light particles can be deduced in a similar manner. We estimate that the multiplicity of Li nuclei associated with the emission of α particles is ≈ 0.2; the multiplicity of carbon ions is about 0.1. Within the uncertainties of this procedure, these multiplicities scale with the integrated cross sections. If we assume that they follow a power law dependence on fragment charge, $M \propto Z^{-1.6}$ (see Fig. 5), and that particles are emitted independently, the total associated multiplicity of fragments with charge $Z \geq 3$ is approximately 0.7, corresponding to the emission of about 12 nucleons in the form of complex fragments. The parametrizations of the single particle cross sections indicate that half of the cross sections are nonequilibrium in nature. Therefore, an appreciable fraction of the available energy and linear momentum are carried away by the emission of nonequilibrium intermediate mass fragments.

The multiplicities of intermediate mass fragments associated with other intermediate mass fragments are deduced from coincidence cross sections between the three heavy ion detectors at $\phi_x = 0°$. The multiplicity of Li fragments associated with Li fragments is approximately 0.2. The C-C multiplicity is approximately 0.1. One must exercise caution in interpreting these results since the estimates are deduced from measurements which are taken over a very restricted angular range. They are, therefore, subject to the effects of momentum conservation and final state interactions between coincident particles. In addition, they are not corrected for probable in-plane enhancements of the coincidence cross sections, which would lower the estimates. Nonetheless, these associated multiplicities are of an order comparable to the multiplicities associated with light particles, suggesting that these fragments do not originate from a peculiar class of reactions with high fragment multiplicities, such as the complete shattering of the target nucleus. Instead, intermediate mass fragments appear to be emitted stochastically with little memory of prior emission.

Complex fragments can also originate from the sequential decay of highly excited projectile residues into two lighter nuclei,[59,60] and this process may contribute to the total fragment cross sections. In this experiment intermediate mass fragments were detected at angles significantly larger than the grazing angle, where such processes might be dominant. Therefore, we cannot estimate the magnitude of contributions from reactions resulting in the forward emission of highly excited projectile residues which subsequently decay by the emission of one complex fragment to larger laboratory angles ($\theta \geq 27°$) and a second fragment to more forward angles. However, the low fragment-fragment multiplicities measured here preclude significant contributions from the decay of primary

TABLE II. The multiplicities M of nonequilibrium light particles associated with intermediate mass fragments of momenta $\langle P_x \rangle$. M_{tot} is the total nucleon multiplicity; $\langle P \rangle$ and $\langle E \rangle$ are the average total momentum and the average total energy carried away by nonequilibrium light particles. Momenta and energies are given in units of MeV/c and MeV, respectively.

	Li			B				C		
$\langle P_x \rangle$ (MeV/c)	820	1080	1350	832	1140	1430	1720	1160	1450	1750
$M_{p,n}$	2.0	1.8	1.7	1.7	2.1	2.0	1.8	1.9	2.0	1.9
M_d	0.5	0.4	0.4	0.5	0.5	0.5	0.4	0.5	0.5	0.5
M_t	0.3	0.2	0.2	0.2	0.3	0.2	0.2	0.2	0.3	0.2
M_α	1.2	1.1	0.9	1.0	1.2	1.2	1.1	1.2	1.3	1.2
M_{tot}	10.4	9.5	8.3	9.1	10.8	10.5	9.4	10.4	11.1	10.1
$\langle P \rangle$ (MeV/c)	1170	1070	940	1030	1220	1180	1060	1170	1250	1140
$\langle E \rangle$ (MeV)	167	152	136	145	174	168	150	165	177	161

projectile residues which were originally emitted at angles larger than about 30°.

The total fragment production cross section is approximately 1.5 b. If we assume that fragment emission is statistical, we can write the fragment production cross sections in the form $\sigma_x^{\text{tot}} = M_x \sigma_{\text{IMF}}$, where M_x denotes the multiplicity of particle x, and σ_{IMF} denotes the cross section for that class of reactions in which fragments can be emitted (IMF denotes intermediate mass fragment). We use the parametrizations of Sec. III to estimate the total cross sections $\tilde{\sigma}_x^{\text{tot}}$. Both Li and C fragment data suggest a value for σ_{IMF} of 2 b. For comparison, the geometrical cross section is 2.8 b. We are therefore led to the conclusion that intermediate mass fragments are emitted with modest probabilities from a large class of reactions, representing between 60% and 70% of the total reaction cross section.

In summary, the production of light intermediate mass fragments, $3 \leqq Z_x \leqq 7$, is accompanied by the emission of approximately ten nucleons in nonequilibrium light particles. The multiplicity of intermediate mass fragments, as deduced from coincidence data with both light particles and other intermediate mass fragments, is of the order of 1, with approximately 12 nucleons being emitted in this form. About half of these are nonequilibrium in nature.

VI. COINCIDENCES BETWEEN INTERMEDIATE MASS FRAGMENTS AND HEAVY RECOIL NUCLEI

In this section we discuss the results of coincidence measurements between intermediate mass fragments and targetlike residual nuclei. Since these two particles carry away a major fraction of the total mass, momentum, and energy of the composite system, a kinematic analysis of such coincidences data can place significant constraints on hypothetical reaction mechanisms.

Angular distributions for targetlike residues detected in coincidence with lithium and carbon nuclei emitted at $\theta_1 = 27.5°$ are shown on the left hand side of Fig. 11. These spectra are normalized to represent the probability distributions for the detection of targetlike residues in coincidence with Li and C nuclei in the momentum ranges $P_{\text{Li}} = 960$–1280 MeV/c, $P_{\text{C}} = 1280$–1600 MeV/c, and $P_{\text{C}} = 1920$–2250 MeV/c. The distributions are shown as a function of θ_2, the polar angle of the projection of $\mathbf{v}_2$ onto the reaction plane, where $\mathbf{v}_2$ denotes the velocity of the coincident heavy residue. They exhibit broad maxima, the widths of which are comparable to the angular acceptance of our experiment. The peak positions expected for complete fusion followed by binary decay are indicated by arrows. The observed maxima are located at angles larger than expected for such fusion-fission processes, indicating that the two particles do not carry away the entire projectile momentum.

The location of the maximum $\theta_2^{\max}$ is not solely a function of the momentum of the intermediate mass fragment. This is illustrated in Fig. 12. The upper part of the figure shows angular distributions of recoiling residual nuclei coincident with B nuclei of different momenta. For energies above the exit channel Coulomb barrier, $\theta_2^{\max}$ increases with increasing values of P_1, qualitatively consistent with momentum conservation. However, as P_1 decreases below the Coulomb barrier, $\theta_2^{\max}$ increases again; $\theta_2^{\max}$ is smallest for emission at the Coulomb barrier. Fragment energies less than the Coulomb barrier can be generated by the sequential particle decay of heavier particle unstable nuclei which were originally emitted with Coulomb barrier energies.[37] The increase of $\theta_2^{\max}$ at momenta below the Coulomb barrier may be caused by such sequential decay processes for which the laboratory velocities of the parent nuclei are, on the average, larger than those of the detected daughter nuclei. Similar observations hold true for other outgoing nuclei. They are in qualitative agreement with the trends measured[36] for ^{14}N induced reactions on Ag at $E/A = 35$ MeV.

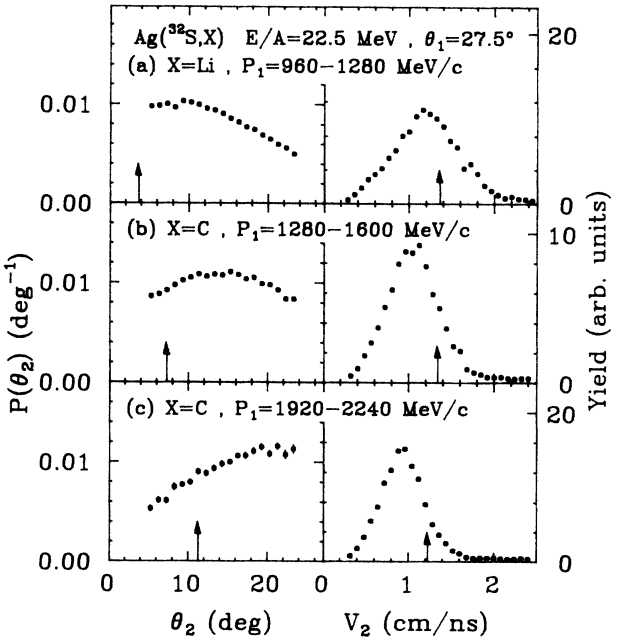

FIG. 11. Velocity distributions for heavy recoil nuclei detected in coincidence with intermediate mass fragments emitted at $\theta_1 = 27.5°$. The left hand side shows the distribution as a function of the polar angle θ_2 of the projection of the recoil velocity onto the reaction plane. The right hand side shows the measured distributions of $|\mathbf{v}_2|$. The arrows show the values expected for binary reactions.

The bottom section of Fig. 12 shows angular distributions for residues coincident with different nuclei of similar momenta. The value of $\theta_2^{\max}$ depends not only on the momentum of the outgoing fragments but also on their mass. This effect is, at least in part, due to the nonmonotonic momentum dependence near the Coulomb barrier, which occurs at different momenta for different fragments. The angular distributions for heavier fragments, $Z_f \geqq 9$, do not exhibit maxima within the angular acceptance of our detector.

Recent results[16] for the ^{84}Kr+^{12}C system at $E/A = 35$ MeV were interpreted in terms of complete fusion followed by binary fragment emission. For the present reaction, the peaks in the angular distributions of the recoiling residues never occur at the angles expected for complete fusion followed by binary decay. This includes reactions

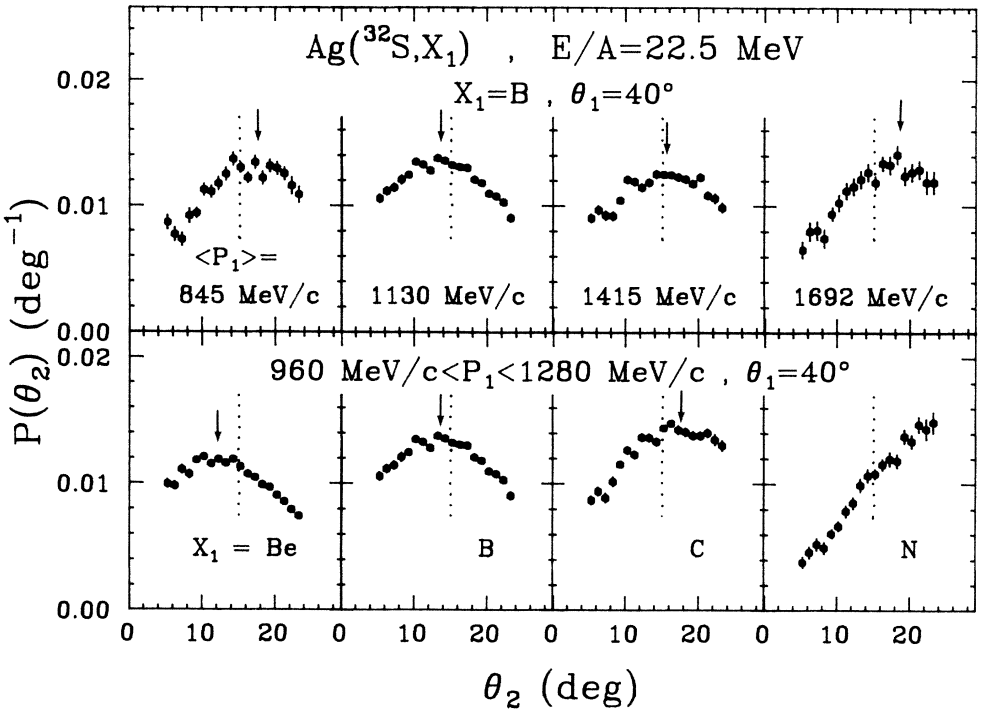

FIG. 12. Probability distributions of recoil nuclei as a function of recoil angle θ_2 detected in coincidences with boron fragments of different momenta P_1 detected at $\theta_1=40°$ (upper part) and in coincidence with different intermediate mass fragments gated by the same momentum bin (lower part). The arrows indicate the angles, $\theta_2^{\max}$, used in the kinematic analysis. The dotted lines correspond to an angle of $\theta_2=15°$.

producing fragments with masses comparable to the mass of the projectile.

We have extrapolated the measured angular distributions to estimate the probability that a heavy residue is emitted in coincidence with an intermediate mass fragment. For this purpose, we have assumed that the distribution is a Gaussian function of angle and that the widths both in-plane and out-of-plane are the same. For the case of carbon nuclei detected at $\theta=27.5°$ with momenta between 1280 and 1600 MeV/c, the width of the distribution in the reaction plane is approximately 25°. Such a narrow distribution is, by itself, inconsistent with an intermediate mass fragment multiplicity significantly greater than 1. The integrated probability for detecting a residue over the measured angular range $\theta=9.5°$–$21.5°$ is about 0.13. Extrapolation over the full angular range gives approximately unit probability for the detection of a coincident heavy residue: The average number of heavy recoil nuclei is approximately 1, consistent with the existence of a single targetlike residue remaining after fragment emission.

Velocity distributions of coincident heavy residues are shown on the right hand side of Fig. 11. They, too, are inconsistent with fusion-fission processes. (The velocities expected for purely binary reactions are indicated by arrows.) There are two sources for systematic errors in the velocity distributions. The first source of uncertainty is due to the energy loss of the residue in the target, which reduces the velocity by 5–10%, depending on the (unknown) mass of the residue. The second source of uncertainty results from the finite angular acceptance of the detector used in this experiment. This effect, discussed in the Appendix, results in an apparent increase in the residue velocity which can be of the order of 10%. Within the uncertainties inherent in making corrections for either effect, the two effects tend to cancel. Therefore, no corrections have been made to the velocity distributions.

For our kinematic analysis we assume that the mass number M_1 of an intermediate mass fragment of charge Z_1 is given by $M_1=2Z_1$. Then, the momentum of the intermediate mass fragment is calculated from the expression

$$\mathbf{P}_1=\hat{\mathbf{P}}_1(2M_1E_1)^{1/2}\,, \tag{7}$$

where $\hat{\mathbf{P}}_1$ is the unit vector characterizing the momentum of the outgoing intermediate mass fragment. The momentum of the heavy residue is given by

$$\mathbf{P}_2(M_2)=\mathbf{v}_2M_2\,, \tag{8}$$

where $\mathbf{v}_2$ is the measured velocity of the residue and M_2 is the mass of the residue, which is not measured. We treat this mass as a parameter in the kinematics calculations. For each assumed value of M_2, we calculate the "missing mass," $M_3=M_0-M_1-M_2$, and the "missing momentum," $\mathbf{P}_3=\mathbf{P}_0-\mathbf{P}_1-\mathbf{P}_2$, carried away by undetected particles in the reaction. Here, M_0 and $\mathbf{P}_0$ denote the total mass and momentum in the reaction.

We define the "sum kinetic energy"

$$E_k=\frac{P_1^2}{2M_1}+\frac{P_2^2}{2M_2}+\frac{P_3^2}{2M_3} \tag{9}$$

as the sum of the kinetic energies of the two detected fragments and the kinetic energy corresponding to the motion

of the center of mass of the missing mass. The difference, $E_0 - E_k$, between the projectile energy and the sum kinetic energy may be associated with the energy dissipated into other, "internal," degrees of freedom. Small values of E_k correspond to violent collisions in which a large amount of energy is converted to excitations of internal degrees of freedom. For example, complete fusion followed by symmetric binary fission would result in $E_k = E_1 + E_2 \approx 250$ MeV.

Another quantity of interest is the magnitude of the center-of-mass velocity of the missing mass, $v_3 = |\mathbf{P}_3/M_3|$. For example, values of v_3 close to the projectile velocity would indicate that the missing momentum is carried away by projectile fragments as might be expected for a breakup-fusion process. Information about the linear momentum transfer is provided by $(P_3)_z$, the component of the missing momentum along the beam axis. Finally, we evaluate the polar angle of the missing momentum, $\theta_3 = \cos^{-1}[(P_3)_z/P_3]$. In our sign convention for this angle, negative angles correspond to the side of the beam opposite the intermediate mass fragments.

As a specific example, we discuss the kinematics for coincidences between heavy recoil nuclei and carbon nuclei, the latter being detected at $\theta_1 = 27.5°$ and with momenta between 1280 and 1600 MeV/c, corresponding to laboratory energies of about 90 MeV. The experimental distributions for this case are shown in Fig. 11(b). The maxima of the angular and velocity distributions are located at $\theta_2^{\max} = 14°$ and $v_2^{\max} = 1.05$ cm/ns, respectively. Calculations of the kinematic quantities defined above were performed as functions of M_2; they are shown as solid curves in Fig. 13.

We may consider undetected light particles evaporated from the heavy residue as part of the mass M_2, because velocities and emission angles of these particles are, on the average, the same as those of the heavy residue. With M_2 defined in this manner, the "missing momentum" is principally due to nonequilibrium emission mechanisms. In Sec. V we have shown that nonequilibrium light particle emission carries away about 10 mass units. Furthermore, there is a non-negligible probability for nonequilibrium emission of nucleons in the form of heavier particles. The average value of M_2 should, therefore, be smaller than 120 by several mass units. We confine our discussion to values of $M_2 < 120$.

The sum kinetic energies E_k extracted from the kinematics analysis are shown in Fig. 13(a). The values of $E_k \approx 200$–300 MeV indicate that amounts of energy between 400 and 500 MeV are dissipated into degrees of freedom other than the nine translational degrees of freedom which are included in the definition of the sum kinetic energy. An energy of approximately 100 MeV is estimated to be associated with the random motion of nonequilibrium light particles. It is possible that a comparable amount of energy is carried away by additional intermediate mass fragment emission. Thus, an amount of energy between 200 and 400 MeV is deposited into internal excitations of the residual nucleus or emitted fragments. Intermediate mass fragments are emitted in highly inelastic collisions.

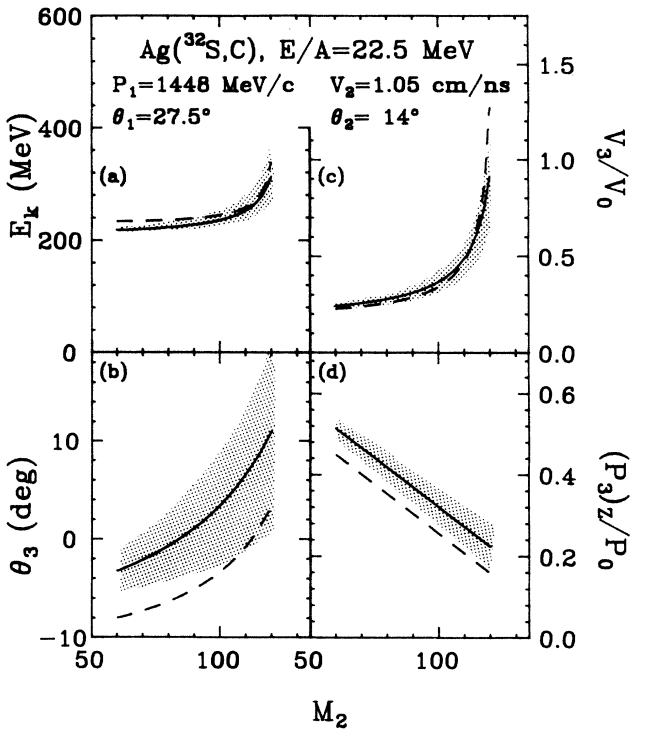

FIG. 13. The solid curves show the results of kinematics calculations for coincidences between heavy recoil nuclei and carbon nuclei, detected at $\theta = 27.5°$ with an average momentum of 1448 MeV/c. The hatched area represents the estimated uncertainties. The dashed curves are obtained when the carbon nucleus is assumed to be a secondary fragment produced by the decay of a particle unstable ^{16}O nucleus. A detailed discussion is given in the text.

The angle of the missing momentum vector is shown in Fig. 13(b). The missing momentum is directed close to the beam axis. The velocity of the missing mass, shown in Fig. 13(c), is less than or equal to the beam velocity. A value of about half the beam velocity, characteristic of pre-equilibrium light particle emission, is consistent with a pre-evaporation residue mass of about 110 mass units and the emission of 15–20 nucleons at the early stages of the reaction. This number is consistent with our estimates of the associated particle multiplicities discussed in Sec. V. The magnitude of the missing momentum is greater than 20% of the projectile momentum; see Fig. 13(d). This value of the missing momentum is slightly larger than the value of the missing momentum, $\approx 15\%$, expected from the systematics of linear momentum transfer measurements for fusionlike reactions.[35] This difference could be explained if one assumed that a significant fraction of the observed fragments correspond to secondary decay products of highly excited primary fragments; this possibility is discussed further below.

In order to assess the sensitivity of the extracted quantities to uncertainties of our input parameters we have varied three of the input parameters separately: the direction of the residue was changed by $\pm 4°$, corresponding to the uncertainty in the most probable recoil angle; the velocity was changed by $\pm 10\%$, corresponding to the uncer-

TABLE III. The observed and calculated kinematic properties of systems for which a heavy residue with a velocity v_2 was detected in coincidence with an intermediate mass fragment with a momentum $\langle P_1 \rangle$ at an angle θ_1.

Z_1	$\langle P_1 \rangle$ (MeV/c)	v_2^{max} (cm/ns)	θ_2^{max}	P_3 (MeV/c)	θ_3	E_k (MeV)
			$\theta_1=27.5°$			
Li	820	1.20	−5.5	1740	0.6	209
Li	1080	1.20	−9.5	1550	6.7	240
Li	1350	1.20	−12.5	1380	11.4	286
Be	836	1.10	−8.5	2100	4.7	223
Be	1110	1.10	−8.5	1850	1.4	234
Be	1400	1.10	−12.5	1640	6.0	266
Be	1680	1.15	−15.0	1280	11.0	305
B	832	1.10	−17.5	2350	18.7	254
B	1140	1.10	−11.5	1870	7.0	232
B	1430	1.05	−13.0	1790	4.9	258
B	1720	1.05	−15.5	1580	6.2	287
B	2010	1.05	−16.5	1330	4.2	326
C	1160	1.10	−16.0	1970	14.9	245
C	1450	1.05	−14.0	1800	6.6	252
C	1740	1.00	−17.0	1750	6.6	283
N	1460	1.10	−17.5	1740	15.5	251
N	1760	1.05	−17.5	1600	9.9	265
N	2060	0.95	−17.5	1630	1.2	302
O	1770	1.05	−19.5	1650	13.7	271
O	2070	1.00	−20.0	1520	8.3	288
			$\theta_1=40°$			
Li	801	1.25	−9.0	1720	5.3	212
Li	1060	1.25	−12.0	1570	7.8	244
Li	1340	1.30	−15.0	1270	13.6	291
Be	833	1.20	−11.5	1910	8.6	217
Be	1100	1.20	−12.0	1700	5.0	234
Be	1380	1.20	−17.0	1600	11.5	272
B	845	1.25	−17.5	1970	22.3	232
B	1130	1.20	−13.5	1710	8.0	229
B	1420	1.15	−15.5	1680	5.0	258
B	1690	1.15	−18.5	1540	6.3	291
C	1160	1.25	−17.5	1680	19.1	233
C	1430	1.20	−17.0	1560	10.6	245
C	1730	1.10	−20.0	1700	6.2	288
N	1440	1.25	−19.5	1510	19.8	244
N	1740	1.15	−21.0	1580	10.9	274
O	1460	1.25	−21.0	1560	22.6	254
O	1750	1.20	−23.0	1520	18.8	272
			$\theta_1=52.5°$			
Li	777	1.25	−9.5	1860	2.9	220
Li	1040	1.30	−15.5	1680	12.8	255
Be	820	1.25	−11.0	1860	5.2	218
Be	1080	1.20	−14.0	1920	4.2	250
Be	1360	1.25	−18.0	1680	8.5	281
B	848	1.35	−15.0	1660	18.6	216
B	1110	1.25	−14.0	1740	5.3	235
B	1390	1.20	−18.0	1810	5.4	273
C	1140	1.30	−16.5	1640	13.0	234
C	1420	1.25	−18.0	1640	7.2	258
N	1150	1.40	−20.0	1530	28.5	241
N	1420	1.30	−20.0	1560	14.9	255
O	1440	1.45	−23.0	1360	36.0	261
O	1730	1.35	−21.0	1220	13.8	261

tainty in the most probable recoil velocity; the mass of the carbon ion was changed by ± 2 amu. The shaded regions in Fig. 13 indicate the range of values of the calculated quantities which result from variations of these parameters. The main results of our analysis are not very sensitive to uncertainties in the input parameters.

Analyses of the coincidence measurements for other intermediate mass fragments or for different fragment momenta lead to similar conclusions. Table III shows measured recoil momenta and directions for which a value of $\theta_2^{\max}$ could be determined. Also, we provide values of the inferred kinematic quantities assuming that $M_2 = 110$.

It is possible that the detected intermediate mass fragments are the decay products of highly excited primary fragments.[51–53] Contributions from such sequential decays are expected to be particularly large for fragment energies below the Coulomb barrier. Indeed, the missing momenta for low energy fragments of $Z = 5$–8 indicate the preferential emission of matter to that side of the beam axis at which these fragments are detected. Part of this emission could be caused by sequential decays of highly excited primary fragments. If we wish to exclude the momenta of the undetected products of sequential decay from the missing momentum, $\mathbf{P}_3$, we have to include them in the definition of $\mathbf{P}_1$, which is then interpreted as the momentum of the primary fragment. To estimate the effect of sequential decay on the total missing momentum, we have assumed that the undetected sequential decay products are emitted with the same average velocity as the detected fragment. The dashed curves in Fig. 13 were obtained by assuming that carbon nuclei resulted from the decay of primary oxygen fragments. From the figure it is clear that sequential decay has a larger influence on the extracted angle of emission and on the longitudinal momentum carried away by the missing mass than it has on E_k and v_3. It is interesting to note that the assumption of sequential decay makes the magnitude of the missing momentum transfer more consistent with the Viola systematics.[35] The inclusion of sequential decay does not, however, change the qualitative results of the kinematic analysis. We may therefore conclude that intermediate mass fragments are produced in reactions in which more than 20% of the incident linear momentum is carried away by nonequilibrium particle emission. These nonequilibrium particles are emitted with a mean velocity which is directed close to the beam axis and which is somewhat less than half of the beam velocity. The reaction is highly inelastic: a total amount of energy between 200 and 400 MeV is dissipated into internal degrees of freedom.

VII. SUMMARY AND CONCLUSIONS

For ^{32}S induced reactions on Ag at $E/A = 22.5$ MeV, the single particle inclusive cross sections of light particles and intermediate mass fragments provide evidence for a gradual transition from predominately nonequilibrium emission of lighter particles to predominantly equilibrium emission for the heaviest nuclei. The integrated cross sections decrease smoothly with fragment mass. There is no evidence for sudden changes in the reaction mechanism.

Intermediate mass fragments and nonequilibrium light particles are preferentially emitted in a plane which contains the beam axis, probably corresponding to the plane perpendicular to the entrance channel orbital angular momentum. This implies that fragment production results from collisions with a large range of impact parameters and is not restricted to central collisions, for which less coplanar emission patterns would be expected. The large azimuthal asymmetries emphasize the need to incorporate dynamical aspects of the collision process into models of complex fragment production.

The fragment multiplicities are low, of the order of 1. For the present reaction there is no evidence that violent multifragmentation processes, implied by some models, dominate the emission of intermediate mass fragments. Instead, it appears that fragments are emitted with modest probabilities from a class of reactions representing 60–70 % of the total reaction cross section.

Intermediate mass fragments are emitted in highly inelastic collisions in which a large part of the kinetic energy of the incident projectile is converted into excitations of internal degrees of freedom. However, the dissipated energy is never completely thermalized in the composite system. Significant parts of the incident momentum and energy are carried away by particles emitted in nonequilibrium processes. Much of this is accounted for by the emission of ten or more nonequilibrium light particles. There is, however, a non-negligible probability for the emission of a second intermediate mass fragment.

Some of these observations are qualitatively consistent with the expectations from a variety of statistical calculations.[11,12,14,27–30] However, present model calculations of intermediate mass fragment emission do not incorporate important dynamical effects which might give rise to the observed angular correlations and nonequilibrium emission.

ACKNOWLEDGMENTS

This work was supported by the National Science Foundation under Grant No. HY 83-12245 and by the U.S. Department of Energy under Contract No. DE-AC05-840R21400 with Martin Marietta Energy Systems, Inc. One of us (W.G.L.) acknowledges the receipt of a National Science Foundation Presidential Young Investigator Award.

APPENDIX

Systematic errors in extracting information from the residue velocities can result from a biased sampling of the residue velocity distribution by a detector with a small angular acceptance. Consider a distribution in $\mathbf{v}$ characterized by a mean velocity $\mathbf{v}_0$ such that $\mathbf{v} = \mathbf{v}_0 + \mathbf{v}'$. For simplicity, we assume that the distribution of $\mathbf{v}'$, $f(\mathbf{v}')$, depends only on v' so that $f(\mathbf{v}') = f(v')$.

By definition, the average velocity for all particles is

$$\langle \mathbf{v} \rangle_{4\pi} = \mathbf{v}_0 \, .$$

However, for a finite detector solid angle in the laboratory, Ω, the measured average is given by

$$\langle \mathbf{v} \rangle_{\Omega} = \frac{\int_{\Omega^+} \mathbf{v} f(v') dv' d\Omega' + \int_{\Omega^-} \mathbf{v} f(v') dv' d\Omega'}{\int_{\Omega^+} f(v') dv' d\Omega' + \int_{\Omega^-} f(v') dv' d\Omega'} \, ,$$

where Ω^+ and Ω^- denote the solid angles corresponding to the two kinematic solutions for values of $\mathbf{v}'$. In general, the measured average is different from $\mathbf{v}_0$.

As an illustration, we assume $f(v')=\delta(v'-a)$. If the detector is centered about $\hat{\mathbf{v}}_0$ and detects all particles emitted inside a cone of half angle α, we can calculate the average velocity of the detected particles,

$$\langle \mathbf{v} \rangle_\Omega = \mathbf{v}_0 \left[1 + \frac{a}{2v_0} \left[\frac{\cos^2\theta - \cos^2\theta_+}{2 - \cos\theta_+ + \cos\theta_-} \right] \right],$$

with

$$\theta_\pm = \cos^{-1} \left\{ -\frac{v_0}{a}\sin^2\alpha \pm \cos\alpha \left[1 - \left[\frac{v_0}{a} \right]^2 \sin^2\alpha \right]^{1/2} \right\}.$$

Here, θ_+ and θ_- represent the angular limits of the solid angles of Ω', Ω^+, and Ω^-. For $a=0.25v_0$, the average emission angle in the laboratory is approximately 16°, similar to that of the experimental distributions. For an acceptance angle of $\alpha=6°$, the measured average velocity is $\langle v \rangle = 1.1v_0$. Calculations with more reasonable distributions as $f(v)$ indicate that values of $\langle v \rangle / v_0 \approx 1.05-1.1$ can be expected for our measured distributions.

---

*Present address: Massachusetts Institute of Technology, Cambridge MA 02139.

†Present address: Institute for Nuclear Studies, 05-400 Swierk N. Warsaw, Poland.

[1]E. K. Hyde, G. W. Butler, and A. M. Poskanzer, Phys. Rev. C **4**, 1759 (1971).

[2]A. M. Poskanzer, G. W. Butler, and E. K. Hyde, Phys. Rev. C **3**, 882 (1971).

[3]G. D. Westfall, R. G. Sextro, A. M. Poskanzer, A. M. Zebelman, G. W. Butler, and E. K. Hyde, Phys. Rev. C **17**, 1368 (1978).

[4]R. E. L. Green and R. G. Korteling, Phys. Rev. C **22**, 1594 (1980).

[5]R. W. Minich, S. Agarwal, A. Bujak, J. Chuang, J. E. Finn, L. J. Gutay, A. S. Hirsch, N. T. Porile, R. P. Scharenberg, B. C. Stringfellow, and F. Turkot, Phys. Lett. **118B**, 458 (1982).

[6]J. E. Finn, S. Agarwal, A. Bujak, J. Chuang, L. J. Gutay, A. S. Hirsch, R. W. Minich, N. T. Porile, R. P. Scharenberg, B. C. Stringfellow, and F. Turkot, Phys. Rev. Lett. **49**, 1321 (1982).

[7]A. S. Hirsch, A. Bujak, J. E. Finn, L. J. Gutay, R. W. Minich, N. T. Porile, R. P. Scharenberg, B. C. Stringfellow, and F. Turkot, Phys. Rev. C **29**, 508 (1984).

[8]A. I. Warwick, H. H. Wieman, H. H. Gutbrod, M. R. Maier, J. Peter, H. G. Ritter, H. Stelzer, F. Weik, M. Freedman, D. J. Henderson, S. B. Kaufman, E. P. Steinberg, and B. D. Wilkins, Phys. Rev. C **27**, 1083 (1983).

[9]K. A. Frankel and J. D. Stevenson, Phys. Rev. C **23**, 1511 (1981).

[10]B. Jakobsson, G. Jönsson, B. Lindkvist, and A. Oskarsson, Z. Phys. A **307**, 293 (1982).

[11]C. B. Chitwood, D. J. Fields, C. K. Gelbke, W. G. Lynch, A. D. Panagiotou, M. B. Tsang, H. Utsunomiya, and W. A. Friedman, Phys. Lett. **131B**, 289 (1983).

[12]L. G. Sobotka, M. L. Padgett, G. J. Wozniak, G. Guarino, A. J. Pacheco, L. G. Moretto, Y. Chan, R. G. Stokstad, I. Tserruya, and S. Wald, Phys. Rev. Lett. **51**, 2187 (1983).

[13]B. V. Jacak, G. D. Westfall, C. K. Gelbke, L. H. Harwood, W. G. Lynch, D. K. Scott, H. Stöcker, M. B. Tsang, and T. J. M. Symons, Phys. Rev. Lett. **51**, 1846 (1983).

[14]D. J. Fields, W. G. Lynch, C. B. Chitwood, C. K. Gelbke, M. B. Tsang, H. Utsunomiya, and J. Aichelin, Phys. Rev. C **30**, 1912 (1984).

[15]R. Trockel, K. D. Hildenbrand, U. Lynen, W. F. J. Mueller, H. J. Rabe, H. Sann, H. Stelzer, R. Wada, N. Brummund, R. Glasow, K. H. Kampert, R. Santo, D. Pelte, J. Pochodzalla, and E. Eckert, Report No. GSI-85-45, Sept. 1985.

[16]W. Mittig, A. Cunsolo, A. Foti, J. P. Wieleczko, F. Auger, B. Berthier, J. M. Pascaud, J. Québert, and E. Plagnol, Phys. Lett. **154B**, 259 (1985).

[17]A. D. Panagiotou, M. W. Curtin, H. Toki, D. K. Scott, and P. J. Siemens, Phys. Rev. Lett. **52**, 496 (1984).

[18]M. E. Fisher, Physics (N.Y.) **3**, 255 (1967).

[19]David Boal, Phys. Rev. C **30**, 119 (1984).

[20]J. B. Cumming, Phys. Rev. C **32**, 1445 (1985).

[21]G. Fài and J. Randrup, Nucl. Phys. **A281**, 557 (1982).

[22]M. W. Curtin, H. Toki, and D. K. Scott, Phys. Lett. **123B**, 289 (1983).

[23]D. Hahn and H. Stöcker (unpublished).

[24]J. Aichelin, J. Hüfner, and R. Ibarra, Phys. Rev. C **30**, 107 (1984).

[25]J. Hüfner and H. M. Sommermann, Phys. Rev. C **27**, 2090 (1983).

[26]S. Bohrmann, J. Hüfner, and M. C. Nemes, Phys. Lett. **120B**, 59 (1983).

[27]L. G. Moretto, Nucl. Phys. **A247**, 211 (1975).

[28]D. H. E. Gross, L. Satpathy, Meng Ta-chung, and M. Satpathy, Z. Phys. A **309**, 41 (1982).

[29]W. A. Friedman and W. G. Lynch, Phys. Rev. C **28**, 950 (1983).

[30]L. G. Sobotka, M. A. McMahan, R. J. McDonald, C. Signarbieux, G. J. Wozniak, M. L. Padgett, J. H. Gu, Z. H. Liu, Z. Q. Yao, and L. G. Moretto, Phys. Rev. Lett. **53**, 2004 (1984).

[31]S. Gales, E. Hourani, M. Hussonnois, J. P. Schapira, L. Stab, M. Vergnes, Phys. Rev. Lett. **53**, 759 (1984).

[32]U. Littmark and J. F. Ziegler, *Handbook of Range Distributions for Energetic Ions in All Elements* (Pergamon, New York, 1980).

[33]T. C. Awes, G. Poggi, S. Saini, C. K. Gelbke, R. Legrain, and G. D. Westfall, Phys. Lett. **103B**, 417 (1981).

[34]G. D. Westfall, B. V. Jacak, N. Anantaraman, M. W. Curtin, G. M. Crawley, C. K. Gelbke, B. Hasselquist, W. G. Lynch, D. K. Scott, M. B. Tsang, M. J. Murphy, T. J. M. Symons, R. Legrain, and T. J. Majors, Phys. Lett. **116B**, 118 (1982).

[35]M. Fatyga, K. Kwiatkowski, V. E. Viola, C. B. Chitwood, D. J. Fields, C. K. Gelbke, W. G. Lynch, J. Pochodzalla, M. B. Tsang, and M. Blann, Phys. Rev. Lett. **55**, 1376 (1985).

[36]R. Bougault, D. Horn, C. B. Chitwood, D. J. Fields, C. K. Gelbke, D. R. Klesch, W. G. Lynch, M. B. Tsang, and K. Kwiatkowski, submitted to Phys. Lett.

[37]M. A. Bernstein, W. A. Friedman, and W. G. Lynch, Phys. Rev. C **29**, 132 (1984); **30**, 412(E) (1984).

[38]M. B. Tsang, C. B. Chitwood, D. J. Fields, C. K. Gelbke, D.

R. Klesch, W. G. Lynch, K. Kwiatkowski, and V. E. Viola, Phys. Rev. Lett. **52**, 1967 (1984).

[39]M. B. Tsang, W. G. Lynch, C. B. Chitwood, D. J. Fields, D. R. Klesch, C. K. Gelbke, G. R. Young, T. C. Awes, R. L. Ferguson, F. E. Obenshain, F. Plasil, and R. L. Robinson, Phys. Lett. **148B**, 265 (1984).

[40]W. G. Lynch, L. W. Richardson, M. B. Tsang, R. E. Ellis, C. K. Gelbke, and R. E. Warner, Phys. Lett. **108B**, 274 (1982).

[41]B. E. Hasselquist, G. M. Crawley, B. V. Jacak, Z. M. Koenig, G. D. Westfall, J. E. Yurkon, R. S. Tickle, J. P. Dufour, and T. J. M. Symons, Phys. Rev. C **32**, 145 (1985).

[42]C. B. Chitwood, D. J. Fields, C. K. Gelbke, D. R. Klesch, W. G. Lynch, M. B. Tsang, T. C. Awes, R. L. Ferguson, F. E. Obenshain, F. Plasil, R. L. Robinson, and G. R. Young, Phys. Rev. C, in press.

[43]D. Fox, D. A. Cebra, Z. M. Koenig, J. J. Molitoris, P. Ugorowski, H. Stöcker, and G. D. Westfall, Phys. Rev. C **33**, 1540 (1986).

[44]I. Tanihata, M.-C. Lemaire, S. Nagamiya, and S. Schnetzer, Phys. Lett. **97B**, 363 (1980).

[45]I. Tanihata, S. Nagamiya, S. Schnetzer, and H. Steiner, Phys. Lett. **100B**, 121 (1981).

[46]F. Zarbakhsh, A. L. Sagle, F. Brochard, T. A. Mulera, V. Perez-Mendez, R. Talaga, I. Tanihata, J. B. Carroll, K. S. Ganezer, G. Igo, J. Oostens, D. Woodard, R. Sutter, Phys. Rev. Lett. **46**, 1268 (1981).

[47]W. G. Lynch, C. B. Chitwood, M. B. Tsang, D. J. Fields, D. R. Klesch, C. K. Gelbke, G. R. Young, T. C. Awes, R. L. Ferguson, F. E. Obenshain, F. Plasil, R. L. Robinson, and A. D. Panagiotou, Phys. Rev. Lett. **51**, 1850 (1983).

[48]H. A. Gustafsson, H. H. Gutbrod, B. Kolb, H. Löhner, B. Ludewigt, A. M. Poskanzer, T. Renner, H. Riedesel, H. G. Ritter, A. Warwick, F. Weik, and H. Weiman, Phys. Rev. Lett. **53**, 544 (1984).

[49]C. B. Chitwood, J. Aichelin, D. H. Boal, G. Bertsch, D. J. Fields, W. G. Lynch, M. B. Tsang, J. C. Shillcock, T. C. Awes, R. L. Ferguson, F. E. Obenshain, F. Plasil, R. L. Robinson, and G. R. Young, Phys. Rev. Lett. **54**, 302 (1985).

[50]M. A. Bernstein, W. A. Friedman, W. G. Lynch, C. B. Chitwood, D. J. Fields, C. K. Gelbke, M. B. Tsang, T. C. Awes, R. L. Ferguson, and F. E. Obenshain, F. Plasil, R. L. Robinson, and G. R. Young, Phys. Rev. Lett. **54**, 402 (1985).

[51]J. Pochodzalla, W. A. Friedman, C. K. Gelbke, W. G. Lynch, M. Maier, D. Ardouin, H. Delagrange, H. Doubre, C. Grégoire, A. Kyanowski, W. Mittig, A. Péghaire J. Péter, F. Saint-Laurent, Y. P. Viyogi, B. Zwieglinski, G. Bizard, F. Lefèbvres, B. Tamain, and J. Québert, Phys. Rev. Lett. **55**, 177 (1985).

[52]J. Pochodzalla, W. A. Friedman, C. K. Gelbke, W. G. Lynch, M. Maier, D. Ardouin, H. Delagrange, H. Doubre, C. Grégoire, A. Kyanowski, W. Mittig, A. Péghaire, J. Péter, F. Saint-Laurent, Y. P. Viyogi, B. Zwieglinski, G. Bizard, F. Lefèbvres, B. Tamain, and J. Québert, Phys. Lett. **161B**, 256 (1985).

[53]J. Pochodzalla, W. A. Friedman, C. K. Gelbke, W. G. Lynch, M. Maier, D. Ardouin, H. Delagrange, H. Doubre, C. Grégoire, A. Kyanowski, W. Mittig, A. Péghaire, J. Péter, F. Saint-Laurent, Y. P. Viyogi, B. Zwieglinski, G. Bizard, F. Lefèbvres, B. Tamain, and J. Québert, Phys. Lett. **161B**, 275 (1985).

[54]C. B. Chitwood, C. K. Gelbke, J. Pochodzalla, Z. Chen, D. J. Fields, W. G. Lynch, R. Morse, M. B. Tsang, D. H. Boal, and J. C. Shillcock, Phys. Lett. **172B**, 27 (1986).

[55]G. Caskey, A. Galonsky, B. Remington, M. B. Tsang, C. K. Gelbke, A. Kiss, F. Deak, Z. Seres, J. J. Kolata, J. Hinnefeld, and J. Kasagi, Phys. Rev. C **31**, 1597 (1985).

[56]J. Aichelin and G. Bertsch, Phys. Rev. C **31**, 1730 (1985), and private communication.

[57]G. Bertsch, H. Kruse, and S. Das Gupta, Phys. Rev. C **29**, 673 (1984).

[58]H. Kruse, B. Jacak, and H. Stöcker, Phys. Rev. Lett. **54**, 289 (1985).

[59]M. J. Murphy, S. Gil, M. N. Harakeh, A. Ray, A. G. Seamster, R. Vandenbosch, and T. C. Awes, Phys. Rev. Lett. **53**, 1543 (1984).

[60]T. C. Awes, R. L. Ferguson, R. Novotny, F. E. Obenshain, F. Plasil, V. Rauch, G. R. Young, and H. Sann, Phys. Rev. Lett. **55**, 1062 (1985).

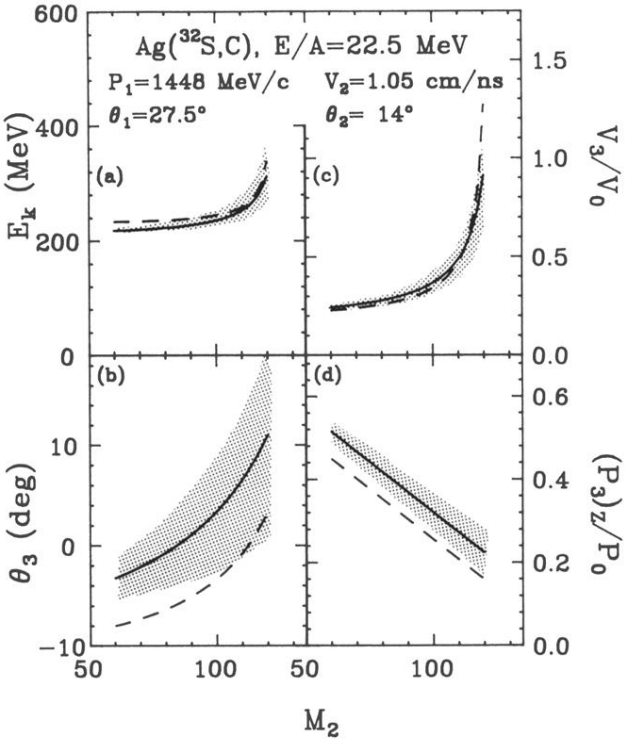

FIG. 13. The solid curves show the results of kinematics calculations for coincidences between heavy recoil nuclei and carbon nuclei, detected at $\theta = 27.5°$ with an average momentum of 1448 MeV/c. The hatched area represents the estimated uncertainties. The dashed curves are obtained when the carbon nucleus is assumed to be a secondary fragment produced by the decay of a particle unstable ^{16}O nucleus. A detailed discussion is given in the text.